Global J. Environ. Sci. Manage. 8(4): 449-472, Autumn 2022, Serial #32

Global Journal of Environmental Science and Management
(GJESM)

Homepage: https://www.gjesm.net/

ORIGINAL RESEARCH ARTICLE

Water quality model-based methodology to assess assimilative capacity of wastewater discharges in rivers

F.M. Torres-Bejarano[1,*], M. Verbel-Escobar[2], M.C. Atencia-Osorio[2]

[1] *Department of Environmental Engineering, University of Córdoba, Carrera 6 No. 77- 305, Montería, Colombia*

[2] *Environmental Engineering Program, University of Córdoba, Carrera 6 No. 77- 305, Montería, Colombia*

ARTICLE INFO

Article History:
Received 19 September 2021
Revised 27 December 2021
Accepted 29 January 2022

Keywords:
Environmental modeling
Hydrodynamics
Pollutant transport
Self-purification
Water resource management

DOI: 10.22034/gjesm.2022.04.01

ABSTRACT

BACKGROUND AND OBJECTIVES: One of the negative impacts of polluting activities on aquatic ecosystems is the loss of its natural self-purification ability, for this reason, the purpose of this research was to evaluate the Sinú River capacity to assimilate wastewater discharges.
METHODS: Monitoring of several water quality parameters was carried out in the river at different seasons and a numerical method was used to simulate different scenarios through the Environmental Fluid Dynamics Code model. The model calibration process was tested applying the Root Mean Square Error and after calibrating the model, scenarios of increase and decrease of discharge concentrations and flows, and river flows were simulated. Finally, the results were compared to water quality reference limits.
FINDINGS: Results show that the model accurately represented the real conditions of the studied river section for all the evaluated parameters. Also, assimilative capacity was affected mostly by the scenario in which the river flow was decreased by 50%, and the flows and discharges concentrations were increased five times; causing parameters such as ammonia nitrogen, chemical oxygen demand, phosphates, and total nitrogen, to exceed the established reference limits with maximum concentrations of 2.7 mg/L, 30.9mg/L, 0.98 mg/L and 6.3 mg/L; respectively. Higher concentrations of water quality parameters were mostly found in the dry season since lower velocities and river flows promote less pollutants mixing and dilution processes.
CONCLUSION: The model spatiotemporal simulations showed the effect of the wastewater discharges on the Sinú River assimilative capacity and made it possible to find those scenarios where water quality parameters exceeded the reference limits, becoming an essential tool for water management and the development of strong water quality objectives by stakeholders and environmental authorities.

NUMBER OF REFERENCES	NUMBER OF FIGURES	NUMBER OF TABLES
58	10	6

*Corresponding Author:
Email: *franklintorres@correo.unicordoba.edu.co*
Phone: +573 0056 77648
ORCID: 0000-0003-3144-7289

Note: Discussion period for this manuscript open until January 1, 2023 on GJESM website at the "Show Article".

INTRODUCTION

Water quality is an issue that has been gaining importance for several years, mainly because water pollution is gradually becoming a significant problem in lakes and rivers (Yuceer and Coskun, 2016). According to the 2018 wastewater report published by the International Water Association (IWA), about 80% of all wastewaters is discharged into the world's waterways, where it creates health, environmental and climate risks, which can lead to changes in their assimilative capacity (AC). Knowledge of the impacts that wastewater discharges generate on water resources is essential for their proper management, and hydrodynamic and water quality models are essential tools for studying these impacts, generally based on the assimilation capacity of water sources (Villota-López *et al.,* 2021). Assimilative capacity refers to the natural ability of water bodies to self-purify and/or self-repair, either through dilution and/or dispersion of wastes and pollution without harming the aquatic environment. In addition, it can indicate the maximum dynamic capacity of the number of pollutants that can be accumulated, destroyed, transformed and transferred beyond the volume of the ecosystem without disturbing its normal activity, that is, the controllable pollutant input for each water flow in a river (Kulikova *et al.,* 2018). A negative impact of polluting activities on aquatic ecosystems is the loss of its natural self-purification and/or self-restoration ability, this translates in the decrease of its assimilative capacity (Lee *et al.,* 2017), since this ability allows a natural treatment of wastewaters in rivers (Egbe *et al.,* 2018), it's important to understand through this research how the discharges' flows and concentrations affect Sinú River assimilative capacity and under which conditions would the capacity become ineffective. Assimilative capacity can be determined through water quality studies and modeling; these have been used as a tool for assimilative capacity analysis in different water bodies. Dehghani *et al.* (2020) considered a one-dimensional pollutant transport model to calculate the assimilative capacity of a river. Hashemi *et al.* (2017) also implemented a one-dimensional model using two objective functions (pollutant concentrations and the distance the pollutants are in contact with the river water) to determine the assimilative capacity and dilution flux; finding that the variation of river flow in different seasons can change the assimilative capacity by up to 97%. Obin *et al.* (2021) applied the WASP model to calculate the water environmental capacity of the Lushui River (China) in normal, wet, and dry periods and Cely-Calixto *et al.* (2021) simulated water quality parameters of the Magdalena River (Colombia) with the mathematical model QUAL2K showing the river's tendency to be purified due to its great flow. Most common methods for assimilative capacity analysis include the design of monitoring programs in water bodies that involve statistical analysis of river and discharge flows with water quality parameters concentration and water quality simulation model configuration to estimate assimilative capacity (Gurjar and Tare, 2019; Quinn *et al.,* 2021). Another common method is the simulation of scenarios in which specific water quality limits are exceeded (Novo, 2017; Villota-López *et al.,* 2021); this method, implementing a two-dimensional hydrodynamic and water quality model, was mainly considered in this research as it can be a starting point to develop strong water quality objectives that can be fundamental in water resource management. According to the Environmental Diagnosis of the Sinú River Basin published in 2004 by the Environmental Authority: Regional Autonomous Corporation of the Sinú and San Jorge Valleys (CVS), domestic wastewater generated in the population centers has been identified as the main source of water pollution in the Sinú River basin. Although the natural conditions have changed due to anthropic action, the Sinú River self-purification capacity is able to recover acceptable quality levels for biota, but, due to the accelerated economic and demographic growth of the population, it is necessary to carry out more current studies on the dynamics of wastewater discharges into the river (CVS, 2004). Feria *et al.* 2017 simulated Sinú River water quality applying Streeter and Phelps model to determine its deoxygenation and re-aeration rates, however, there aren't assimilative capacity studies of this river, which is the third most important river in Colombia's Caribbean region. This study aims to assess the Sinú River capacity to assimilate wastewater discharges and its effects on this ability, analyzing through hydrodynamic and water quality modeling a section of the Sinú River, Colombia. This study has been carried out in a section of 11.06 km of the Sinú River, Montería City, Colombia using information from four monitoring campaigns in 2019.

MATERIALS AND METHODS

Description of the study area

Sinú River is the main water source in the Department of Córdoba and the third most important in Colombia on its Caribbean slope. It is born in the Nudo de Paramillo in the municipality of Ituango, Antioquia, and flows into the Caribbean Sea in the Tinajones delta area of San Bernardo del Viento, Córdoba. It has an extension of 437.97 km and about 13952 km^2 of watershed (CVS, 2004). In its course through the department of Córdoba, the Sinú River irrigates 16 municipalities, among which is the departmental capital, the city of Montería, which is crossed by the river in its middle reaches, where it becomes meandering with an alluvial plain composed of flood plains, with an average temperature of 27.17 °C (Valbuena, 2017). Monteria's total annual average rainfall is 1262 mm. The dry period goes from the beginning of December until mid- or late April. The wet period begins in May and ends in early December, with a tendency of decreasing rainfall in July and August (transition period); most of the rain falls in September, October, and November. The selected section of the Sinú River for this study has an extension of approximately 11.06 km, is located in Montería city (Colombia), and includes the route from Sierra Chiquita (8°44'11.16"N and 75°54'35.08"W) to the University of Córdoba (8°47'27.08"N and 75°51'47.10"W), as shown in Fig. 1. Along the study section, the Sinú River receives continuous discharges of domestic wastewater from communities settled along its banks, most of which are not authorized by the competent environmental authority. It also receives discharges from other informal activities (vehicle washing, among others) and authorized discharges from the treatment plants of Montería city (WWTP Northeastern and WWTP Southwestern).

Data collection

Information on hydrodynamic and climatic variables (flow rates, levels, precipitation, solar radiation, air temperature, wind speed and direction, and relative humidity) was downloaded from the Hydrology and Meteorology Data Management Information System (DHIME) developed by the Institute of Hydrology, Meteorology and Environmental Studies (IDEAM)

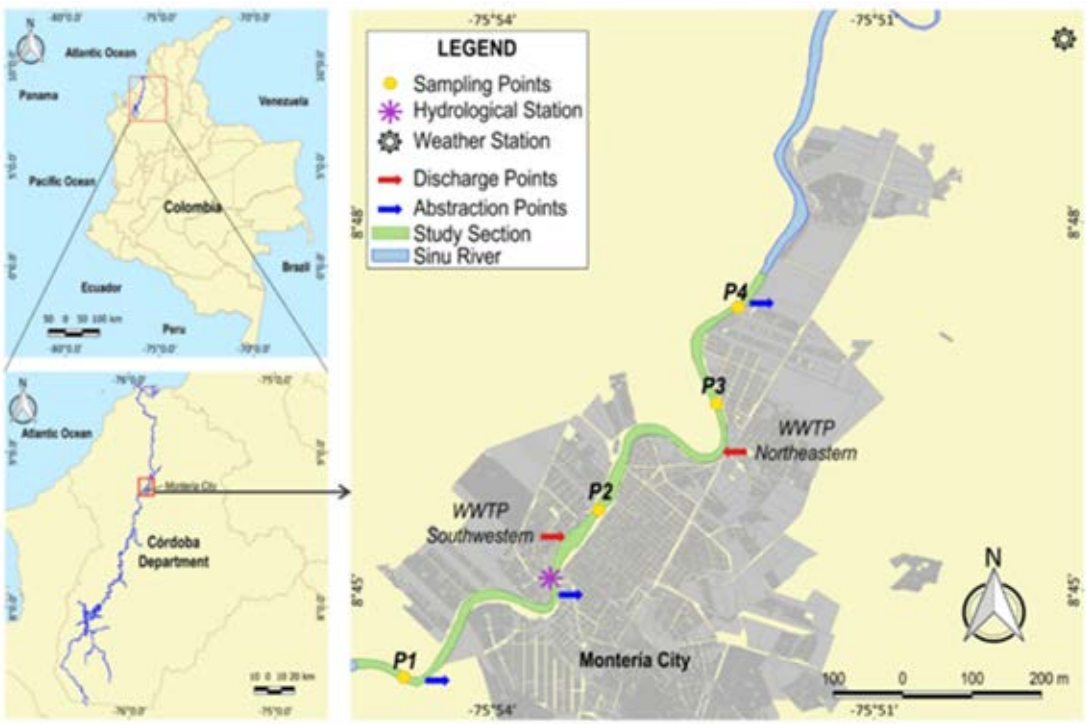

Fig. 1: Geographic location of the study area and sampling locations in the Sinú River section through Monteria city, Colombia

from the following stations:

1) Montería - Automatic (Aut) Station [13067020, Hydrological]: 8°45'05.8"N - 75°53'32.7"W.
2) Los Garzones Airport Station [13035501, Meteorological]: 8°49'33.0"N - 75°49'30.5"W.

In addition, the CVS provided information on the abstraction points (flow rates granted) and discharge points (flow rates and physicochemical characterization) within the study reach.

Water samples were collected during four monitoring campaigns in 2019 (March 18th, July 18th, September 25th and October 31st), for four points established along the study section (Fig. 1), collecting a total of 16 samples to obtain water quality data of the river and be able to carry out the model's calibration. Each point was defined considering the IDEAM (2017) Water Monitoring Protocol and was duly georeferenced with a Garmin GPS 60CSx. Temperature (T) and dissolved oxygen (DO) were measured *in situ* using a HANNAH Multiparameter Probe (model HI-929829), while water samples were studied taking into consideration the general techniques and preservation of sampling of the NTC-ISO 5667 for laboratory analysis of total nitrogen (TN) [SM 4500-Norg B; 4500-NH3 C], ammonia nitrogen (NH3-N) [SM 4500-NH3 B; SM 4500-NH3 C], phosphates (PO4-P) [SM 4500-P E], chemical oxygen demand (COD) [SM 5220 C] and total suspended solids (TSS) [SM 2540 D]. Furthermore, a monitoring campaign was carried out in May 2019 where depth data were taken along the study section to generate the river bathymetry utilizing a Garmin ECHOMAP 73sv bathymetric depth sounder.

Numerical model description

Initially developed at the Virginia Institute of Marine Science (VIMS) and subsequently sponsored by the United States Environmental Protection Agency (US EPA) and the National Oceanic and Atmospheric Administration (NOAA) Sea Grant Program, the Environmental Fluid Dynamics Code (EFDC) is a multifunctional surface water modeling system that can be used to simulate aquatic systems in one, two and three dimensions and includes hydrodynamic components, sediment contaminants and eutrophication. It can also simulate the transport of water quality constituents in geometrically and dynamically complex water bodies such as rivers, stratified estuaries, lakes, and coastal seas. It solves the motion (vertically hydrostatic) and free surface equations, along with the continuity and mass balance equations, i.e., with coupled hydrodynamics, salinity, temperature, sediment, and contaminant transport modules. It also allows drying and wetting in shallow areas employing a massive conservation scheme (Torres-Bejarano *et al.*, 2016; Ramos, 2018). Yiping *et al.* (2011) used it to study the impacts of water transfer on the transport of dissolved substances in Taihu Lake using the water age concept. Kim *et al.* (2017) used it to model algal bloom occurrence atterns in the lower part of this Han River to understand algal dynamics to better develop management alternatives. And Villota-López *et al.* (2021), to estimate the assimilative capacity of the Gallinas River. The water quality simulations and assimilative capacity was evaluated using the EFDC Explorer 10.2.2 modeling system, a commercial version of EFDC developed by DSI Company.

Hydrodynamics and water quality modules

EFDC Explorer applies hydrodynamic modeling based on the turbulent equations of motion and utilizing the Boussinesq approximation for variable density (variable density is a strictly mandatory analysis when dealing with equations for compressible flow), resulting in the momentum Eqs. 1 and 2, the continuity equation, the state equation and the transport equations for salinity and temperature, solved integrally in 2D and 3D. For more detailed information on these equations refer to DSI, (2020) and Torres-Bejarano *et. al.* (2020).

The momentum equation in the x direction:

$$\frac{\partial(m_x m_y Hu)}{\partial t} + \frac{\partial(m_y Huu)}{\partial x} + \frac{\partial(m_x Hvu)}{\partial y} + \frac{\partial(m_x m_y wu)}{\partial z} - m_x m_y fHv - \left(v\frac{\partial m_y}{\partial x} - u\frac{\partial m_x}{\partial y} \right) Hv = -m_y H\frac{\partial(g\zeta+p+P_{atm})}{\partial x} - m_y\left(\frac{\partial h}{\partial x} - z\frac{\partial H}{\partial x}\right)\frac{\partial p}{\partial z} + \frac{\partial}{\partial x}\left(\frac{m_y}{m_x}HA_H\frac{\partial u}{\partial x}\right) + \frac{\partial}{\partial y}\left(\frac{m_x}{m_y}HA_H pd[u]y\right) + \frac{\partial}{\partial z}\left(\frac{m_x m_y}{H}A_v\frac{\partial u}{\partial z}\right) - m_x m_y c_p D_p u\sqrt{u^2+v^2} + S_u \quad (1)$$

The momentum equation in the y direction

$$\frac{\partial(m_x m_y \mathrm{Hv})}{\partial \mathrm{t}} + \frac{\partial(\mathrm{m_y Huv})}{\partial \mathrm{x}} + \frac{\partial(\mathrm{m_x Hvv})}{\partial \mathrm{y}} + \frac{\partial(m_x m_y \mathrm{wv})}{\partial \mathrm{z}} - m_x m_y f Hu + \left(\mathrm{v}\frac{\partial \mathrm{m_y}}{\partial \mathrm{x}} - \mathrm{u}\frac{\partial \mathrm{m_x}}{\partial \mathrm{y}}\right) Hu = -m_x \mathrm{H}\frac{\partial(\mathrm{g}\zeta + p + P_{atm})}{\partial \mathrm{y}} - m_x\left(\frac{\partial \mathrm{h}}{\partial \mathrm{y}} - \mathrm{z}\frac{\partial \mathrm{H}}{\partial \mathrm{y}}\right)\frac{\partial \mathrm{p}}{\partial \mathrm{z}} + \frac{\partial}{\partial x}\left(\frac{m_y}{m_x} H A_H \frac{\partial v}{\partial x}\right) + \frac{\partial}{\partial y}\left(\frac{m_x}{m_Y} H A_H \frac{\partial v}{\partial y}\right) + \frac{\partial}{\partial z}\left(\frac{m_x m_y}{H} A_v \frac{\partial v}{\partial z}\right) + m_x m_y c_p D_p v\sqrt{u^2+v^2} + S_v \quad (2)$$

Where, *u, v* are the horizontal velocity components in the curvilinear coordinates; *x, y* are the orthogonal curvilinear coordinates in the horizontal direction; *z* is the sigma coordinate; *t* is time; m_x, m_y are the square roots of the diagonal components of the metric tensor; P_{atm} is the barotropic pressure; $H = h+\zeta$, Total depth, is the sum of depth and free surface; *p* is the physical pressure in excess of the reference density hydrostatic pressure; *f* is the Coriolis parameter; A_H is the horizontal momentum and mass diffusivity; A_v is the vertical turbulent eddy viscosity; c_p is the vegetation resistance coefficient; D_p is the projected vegetation area normal to the flow per unit horizontal area S_u, S_v are the source/sink terms for the horizontal momentum in the *x* and *y* directions, respectively. In Eqs. 1 and 2, the first term from left to right represents the rate of change of velocity with respect to time; the next three are the advective components and represent fluid motion due to inertial forces; the one that follows is the Coriolis acceleration in the curvature and on the tangential stresses of the bottom, represented through the variation of the free surface; the one immediately after the equal sign is the pressure force, represented through the variation of the free surface, and the next two, the viscous forces that give rise to turbulence within the flow. Water quality structure managed by EFDC Explorer model is mainly composed of reactions that occur in water through organic and inorganic cycles, such as nitrogen, chemical oxygen demand, phosphorus, and algae. The governing mass-balance equation for each of the water quality state variables may be expressed as Eq. 3.

Advection-Diffusion-Reaction equation

$$\overbrace{\frac{\partial}{\partial t}(m_x m_y HC)}^{a} + \overbrace{\frac{\partial}{\partial x}(m_y HuC) + \frac{\partial}{\partial y}(m_x HvC) + \frac{\partial}{\partial z}(m_x m_y wC)}^{b} = \overbrace{\frac{\partial}{\partial x}\left(\frac{m_y H A_x}{m_x}\frac{\partial C}{\partial x}\right) + \frac{\partial}{\partial y}\left(\frac{m_x H A_y}{m_y}\frac{\partial C}{\partial y}\right) + \frac{\partial}{\partial z}\left(m_x m_y \frac{A_z}{H}\frac{\partial C}{\partial z}\right)}^{c} + \overbrace{m_x m_y H S_c}^{d} \quad (3)$$

As shown in Eq. 3, *C* is the concentration or intensity of transport constituent; *u, v* are the horizontal velocity components in the curvilinear coordinates; *w* is the vertical velocity component; A_H is the horizontal turbulent eddy diffusivity; S_c is the internal and external sources and sinks per unit volume; *H* is the total water depth. Eq. 3 comprises physical, advective and diffusive transport, together with kinetical processes; *a* is a temporal term, whereas *b* represents advection transport. On the right side, *c* represents the diffusive transport, and *d* is the reaction term which represents both the kinetic processes and external loads for each of the state variables (DSI, 2020; Villota-López *et. al.,* 2021).

Ammonia nitrogen reaction equation

$$\frac{\partial NH_4}{\partial t} = \sum_{x=c,d,g,m}(FNI_x BM_x + FNIP_x PR_x - PN_x P_x)\, ANC_x B_x + K_{DON} DON - K_{Nit} NH_4 + \frac{BFNH_4}{\Delta z} + \frac{WNH_4}{V} \quad (4)$$

In Eq. 4, FNI_x is the fraction of metabolized nitrogen by algal group *x* produced as inorganic nitrogen; *FNIP* is the fraction of predated nitrogen produced as inorganic nitrogen; PR_x is the predation rate of algal group *x;* PN_x is the preference for ammonium uptake by algal group *x*; P_x is the production rate of algal group *x;* ANC_x is the nitrogen-carbon ratio constant in algal group *x*; B_x is the algal biomass of algal group *x*; K_{DON} is the rate of dissolved organic nitrogen mineralization; *DON* is the dissolved organic nitrogen concentration; $BFNH_4$ is the water-sediment ammonium flux exchange, applied only to the bottom of the layer; WNH_4 are the external ammonium loads and K_{Nit} is the nitrification rate.

Reaction equation of total phosphate

Small concentrations of phosphate and other

phosphorus compounds can be found in natural water bodies. These substances leach from the terrain or result from organic pollution. Phosphates are directly linked to eutrophication (DSI, 2020). The equation employed by the model using Eq. 5.

$$\frac{\partial}{\partial t}(PO4t) = \sum_{x=c,d,g,m}(FPI_x(BM_x) + FPIP_x(PR_x) - P_x)APC_x(B_x) + K_{DOP}(DOP) + \frac{\partial}{\partial z}\left(WS_{TSS}(PO4p)\right) + \frac{BFPO4d}{\Delta Z} + \frac{WPO4p}{V} + \frac{WPO4d}{V} \quad (5)$$

Note that in Eq. 5, *PO4t* is the total phosphate concentration; K_{DOP} is the mineralization rate of dissolved organic phosphorus; *PO4p* is the particulate (sorbed) phosphate; *PO4d* is the dissolved phosphate; FPI_x is the fraction of metabolized phosphorus by algal group *x* produced as inorganic phosphorus; BM_x is the basal metabolism rate of algal group *x*; *FPIP* is the fraction of predated phosphorus produced as inorganic phosphorus; *APC* is the mean algal phosphorus-to-carbon ratio for all algal groups; K_{DOP} is the dissolved organic phosphorus mineralization rate; *DOP* is the dissolved organic phosphorus concentration; WS_{TSS} is the settling velocity of the suspended solid, provided by the hydrodynamic model; *BFPO4d* is the sediment-water exchange flux of phosphate, applied to the bottom layer only; *WPO4t* is the external loads of total phosphate, and *V* is the cell volume.

Dissolved oxygen reaction equation

$$\frac{\partial DO}{\partial t} = \sum_{x=c,d,g,m}\left[(1+0.3(1-PN_x))P_x - (1-FCD_x)\left(\frac{DO}{KHR_x+DO}\right)BM_x\right] + AOCR(B_x) - (AONT)(K_{Nit})(NH_4) - AOCR(K_{HR})(DOC) - \left(\frac{DO}{KH_{COD}+DO}\right) + K_{COD}(COD) + K_R(DO_s - D \frac{SOD}{\Delta z} + \frac{WDO}{V} \quad (6)$$

In Eq. 6, FCD_x is the fraction of basal metabolism exuded as dissolved organic carbon; KHR_x is the half-saturation constant of dissolved oxygen for algal dissolved organic carbon excretion for group *x*; *AOCR* is the dissolved oxygen-to-carbon ratio in respiration; *AONT* is the mass of dissolved oxygen consumed per unit mass of ammonium nitrogen nitrified; NH_4 is the ammonium nitrogen concentration; K_{HR} is the heterotrophic respiration rate of dissolved organic carbon; *DOC* is the concentration of dissolved organic carbon; KH_{COD} is the half-saturation constant of dissolved oxygen required for oxidation of *COD*; *DO* is the dissolved oxygen concentration; *COD* is the chemical oxygen demand concentration; K_R is the reaeration coefficient; DO_s is the saturated concentration of dissolved oxygen; *SOD* is the sediment oxygen demand, applied to the bottom layer only, and *WDO* is the external loads of dissolved oxygen.

Chemical oxygen demand reaction equation

$$\frac{\partial COD}{\partial t} = -\left(\frac{DO}{KH_{COD}+DO}\right)K_{COD}COD + \frac{BFCOD}{\Delta z} + \frac{WCOD}{V} \quad (7)$$

As shown in Eq. 7, KH_{COD} is the half-saturation constant of dissolved oxygen required for oxidation of chemical oxygen demand; K_{COD} is the oxidation rate of chemical oxygen demand; *BFCOD* is the sediment flux of chemical oxygen demand, applied to bottom layer only and *WCOD* is the external loads of chemical oxygen demand.

Suspended sediment transport equation

The water column equation for suspended sediment transport is derived from the generic transport Eq. 3 for a dissolved or suspended material. From which the physical terms of horizontal diffusion are omitted due to small inherent numerical diffusion encountered.

$$\frac{\partial}{\partial t}\left(mHC_j\right) + \frac{\partial}{\partial x}\left(PC_j\right) + \frac{\partial}{\partial y}\left(QC_j\right) + \frac{\partial}{\partial z}\left(mwC_j\right) - \frac{\partial}{\partial z}\left(mw_{s,j}C_j\right) = \frac{\partial}{\partial z}\left(m\frac{A_b}{H}\frac{\partial}{\partial z}C_j\right) + S^E_{s,j} + S^I_{s,j} \quad (8)$$

For Eq. 8, *Cj* represents the concentration of the j^{th} sediment class; A_b is the vertical turbulent eddy viscosity (m^2/s); w_s is the settling velocity of the sediment particles; $S^E_{s,j}$ is the external source-sink term, and $S^I_{s,j}$, is the internal source-sink term. The source term has been split into two terms so that the external source-sink term can include both point and non-point source loads. And the internal source-sink term can include the reactive decomposition of organic sediments or the exchange of mass between sediments classes (DSI, 2020).

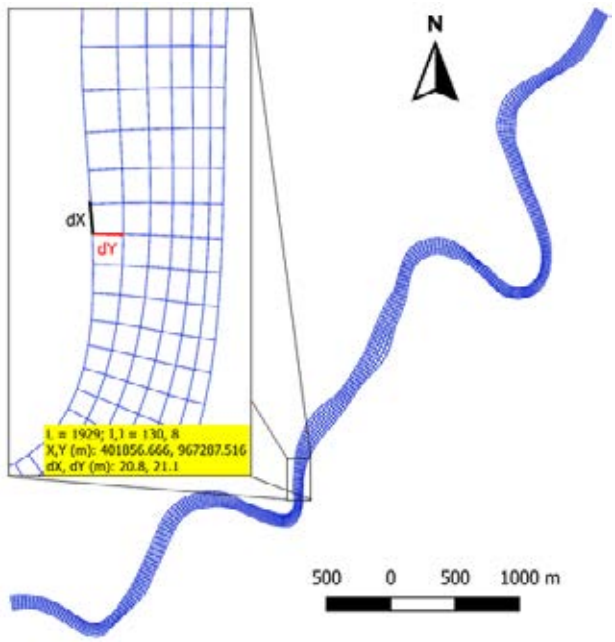

Fig. 2: Configuration of the generated grid

Modeling framework

For purposes of spatial discretization of the model in the study section, a numerical structured grid in a curvilinear and orthogonal system was generated, with a total of 6 rows, 360 columns and 2160 cells whose spacing varies in DX from 10.2 m to 58.3 m and in DY from 8.9 m to 47.03 m, since it presented the best computational times and greater stability during the model calculations (Fig. 2). The bathymetry was processed on this grid, and initial and boundary conditions were included to simulate hydrodynamics and water quality. Subsequently, the model was calibrated to obtain and guarantee reliable results. The simulation period was from February 28th to October 31st, 2019.

Initial and boundary conditions

Absolute depths obtained during the bathymetric campaign were transformed to river bottom elevations using the free water surface level of that day, obtained from the hydrological station Montería – Aut of IDEAM. Meteorological data (solar radiation, air temperature, wind speed and direction, precipitation, evaporation, and relative humidity) were obtained from IDEAM's Los Garzones Airport weather station. The initial water level was established based on the level reported by the Montería - Aut station for the starting day of the simulation (February 28th, 2019). From this same station, river flows were also obtained from a daily time series covering the entire simulation period (Fig. 3). The discharge and abstraction flows were provided by the environmental authority CVS. Dirichlet-type boundaries were defined as inflows referring to the upstream flow of the Sinú River and discharge flows, and outflows referring to abstraction flows. In addition, a free-flow outlet was established at the river's downstream boundary (Neumann-type boundary) (Fig. 3). Sinú River flow in the representative dry season month (March) varies between 125.1 m^3/s and 136.1 m^3/s; in October, the representative wet season month reaches flows up to 709.8 m^3/s. WWTP Northeastern and WWTP Southwestern have a discharge flow of 0.314 m^3/s and 0.099 m^3/s, respectively. Fig. 3 shows river flow input conditions for the whole simulation period.

Initial conditions for each water quality parameter (Fig. 3) were established from *in situ* measurements at the monitoring points (P1 and P4). The parameters concentrations at P1 (Fig. 1) were used as upstream conditions inflow of the Sinú River and the parameters concentrations at P4 (Fig. 1) were used as downstream free boundary conditions. Likewise, the

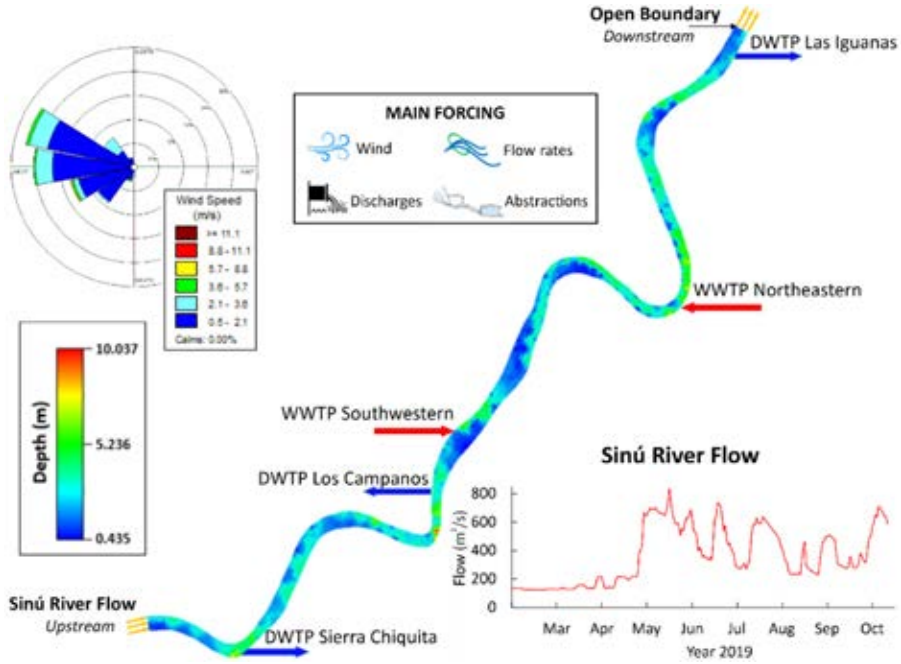

Fig. 3: Initial and boundary conditions

Table 1: WWTP parameters concentrations for water quality simulation

Parameters	WWTP Northeastern	WWTP Southwestern
Temperature (ºC)	30.2	36.2
COD (mg/L)	117.69	142.15
DO (mg/L)	1.9	1.9
NH_3-N (mg/L)	15	15
PO_4-P (mg/L)	3.5	3.5
TSS (mg/L)	68.17	43.56
Flow (m^3/s)	0.314	0.099

concentrations of each of the discharges' parameters were defined according to the information provided by the CVS (Table 1).

Model calibration

The hydrodynamic model was calibrated by gradually adjusting the hydrodynamics coefficients (bottom roughness, horizontal viscosity, etc.) and comparing the simulated water levels with the measured water level data in the river expressed as a time series obtained from the Montería - Aut station during the simulation period. The water quality model was calibrated using the time series generated for each analyzed physicochemical and biological parameter in P2 and P3 (Fig. 1), during the four measurement campaigns. Throughout the calibration process, coefficients and rates of the chemical reactions that govern the behavior of the physicochemical and biological parameters were gradually adjusted. In order to check the fit of the model simulated data with those measured *in situ*, the Root Mean Square Error (RMSE) was applied to measure the amount of error between the two data sets. RMSE ranges from 0 to ∞, where a value equal to 0 indicates a perfect fit using Eq. 9 (Ritter and Muñoz-Carpena, 2013).

$$RMSE = \sqrt{\frac{\sum_{i=1}^{n}(O_i - p_i)^2}{N}} \quad (9)$$

Where, O_i y p_i represent the sample (of size

Table 2: Evaluation criteria for RMSE (Ritter and Muñoz-Carpena, 2013)

Classification	Criteria
Very good	SD ≥3.2RMSE
Good	2.2RMSE≤SD<3.2RMSE
Acceptable	1.2RMSE≤SD<2.2RMSE
Unsatisfactory	SD<1.2RMSE

Standard Deviation (SD) of the measured data.

Table 3: Simulation scenarios applied in Sinú River

Scenario	Description	River	Discharges		
		F (%)	F (%)	Concentrations (%)	
				DO	Others
AS	Actual State of the river discharges and flows.	NC	NC	NC	NC
S1	Discharges' concentration modification.	NC	NC	↓80	↑400
S2	Decrease of river flow.	↓50	NC	NC	NC
S3	Decrease of river flow and discharges concentration modification.	↓50	NC	↓80	↑400
S4	Decrease of river flow and increase of discharges' flows.	↓50	↑400	NC	NC
S5	Decrease of river flow; increase of discharges' flows and modification of its concentrations.	↓50	↑200	↓66.67	↑200
S6		↓50	↑400	↓80	↑400

NC: No change; F: *Flow*; Others: T, COD, NH_3-N, TN, PO_4-P, TSS; ↑: *Increase*; ↓: *Decrease.*

Table 4: Modified coefficients in the hydrodynamic component

Hydrodynamic module	
Parameter	Value
Constant Horizontal Eddy Viscosity (m^2/s)	0.001
Horizontal Momentum Diffusivity (dimensionless)	0.150
Bottom roughness (m)	0.025

N) containing the measured and simulated data, respectively, for cell *i*. Table 2 shows the evaluation criteria for the RMSE.

Modeling scenarios formulation

The scenarios shown in Table 3 were formulated considering the National Water Resource Modeling Guide for inland surface waters. The concentrations of the discharges' parameters in the study section were modified to estimate under what conditions the river would not be able to assimilate the pollutants.

Assimilation capacity

To evaluate the assimilation capacity, the results obtained with the simulated scenarios were compared with the quality criteria applicable to any water body, which, for the case of Colombia, are regulated by the 1076 Decree of 2015 of the Ministry of Environment and Sustainable Development, in articles 2.2.3.3.3.9.2 to 2.2.3.3.3.9.12, and the 2115 Resolution of 2017 of the Ministry of Social Protection. However, these do not contemplate limit values for some parameters such as COD, TSS, NH_3-N, among others; therefore, legislation from countries such as Brazil (Resolution 357 of 2005) and the United States (EPA Standards) was consulted. Based on the current uses in the river, and the regulations and guidelines consulted, the quality criteria that would serve as a guide for the use of the water resource were consolidated.

RESULTS AND DISCUSSION

Hydrodynamic component calibration

The hydrodynamic model was calibrated by comparing the levels obtained from the Montería Aut. Station with the levels calculated by the model. During this process, some hydrodynamic coefficients were adjusted to obtain an optimal calibration (Table 4).

Fig. 4 shows the comparison between the observed

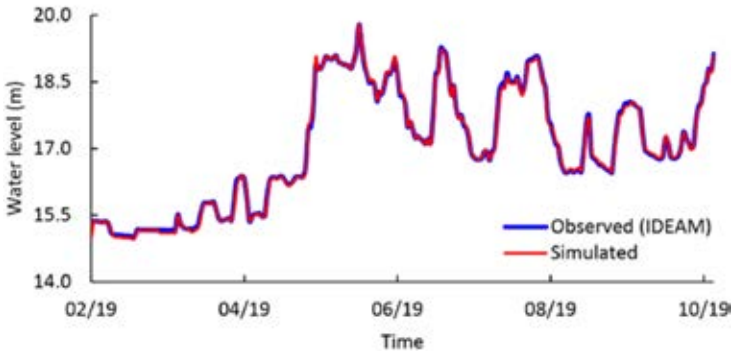

Fig. 4: Hydrodynamic component calibration

data and the simulated data. To verify the fit, the RMSE was calculated, resulting in a value of 0.089, which is in the very good fit category. This indicates that the simulated results are a good representation of the behavior and magnitude of the real levels in the study area during the simulation period.

Water quality component calibration and validation

Fig. 5 shows the results of the calibration of each parameter. The calibration of this module was performed with the concentrations obtained at points P2 and P3; it was necessary to adjust the water quality module coefficients with the values shown in Table 5.

To verify the calibration process, the RMSE was estimated for all simulated parameters (Temperature, COD, DO, NH_3-N, TN, PO_4-P, TSS) at points 2 and 3, considering the standard deviations of the data, the results are shown in Table 6. In P3, parameters such as temperature, PO_4-P and TSS were found in a very good fit category; COD, DO and NH_3-N in an acceptable category and TN in a good fit category. Considering all the calibration results, the EFDC Explorer model reached an accurate representation of the real conditions of the studied river section, which makes very acceptable the simulations of the hydrodynamic and physicochemical processes of the river. The comparison between simulated and measured data also shows that model results follow the seasonal trend seen in field data.

Hydrodynamic simulation

Once the calibration process was completed, the actual state of the study reach was simulated. The results for the dry season were obtained from the representative date of March 31st, and for the wet season, the representative date was October 26th, 2019. Water velocity in rivers can be affected by factors such as river geometry, roughness, slope zones and flow rate. Fig. 6 shows the velocity simulation results for dry and wet seasons. During the dry season (lower flows), velocities were below 0.61 m/s, while in the wet season (higher flows) velocities of up to 0.86 m/s were reached. The spatial changes in velocity in each season are not very significant, because the study section is in an alluvial plain area where slope variations are not representative (CVS, 2004; Acosta, 2013).

Water quality simulation

Results of the water quality simulations for the dry season were also obtained from the representative date of March 31st, and for the wet season the representative date was October 26th, 2019; the results for each parameter are observed in Fig. 7. Regarding the temporal variation, an increase in DO is observed during the wet season, this is consistent with what is reported in the literature, where precipitation has a positive effect on this parameter (Muñoz *et al.*, 2015; Liu *et al.*, 2020). In the case of parameters such as COD, NH_3-N, TN and PO_4-P the highest concentrations were found in the dry season; this occurs because the decrease in flow rates during this season generates a higher concentration of pollutant loads, which causes a decrease in DO and an increase in COD, due to decomposition processes (Liu *et al.*, 2020), additionally, Benjumea *et al.*, (2018) suggest that the high presence of organic matter at lower flow rates does not allow the dilution of nutrients. The highest concentrations of TSS occurred in the wet

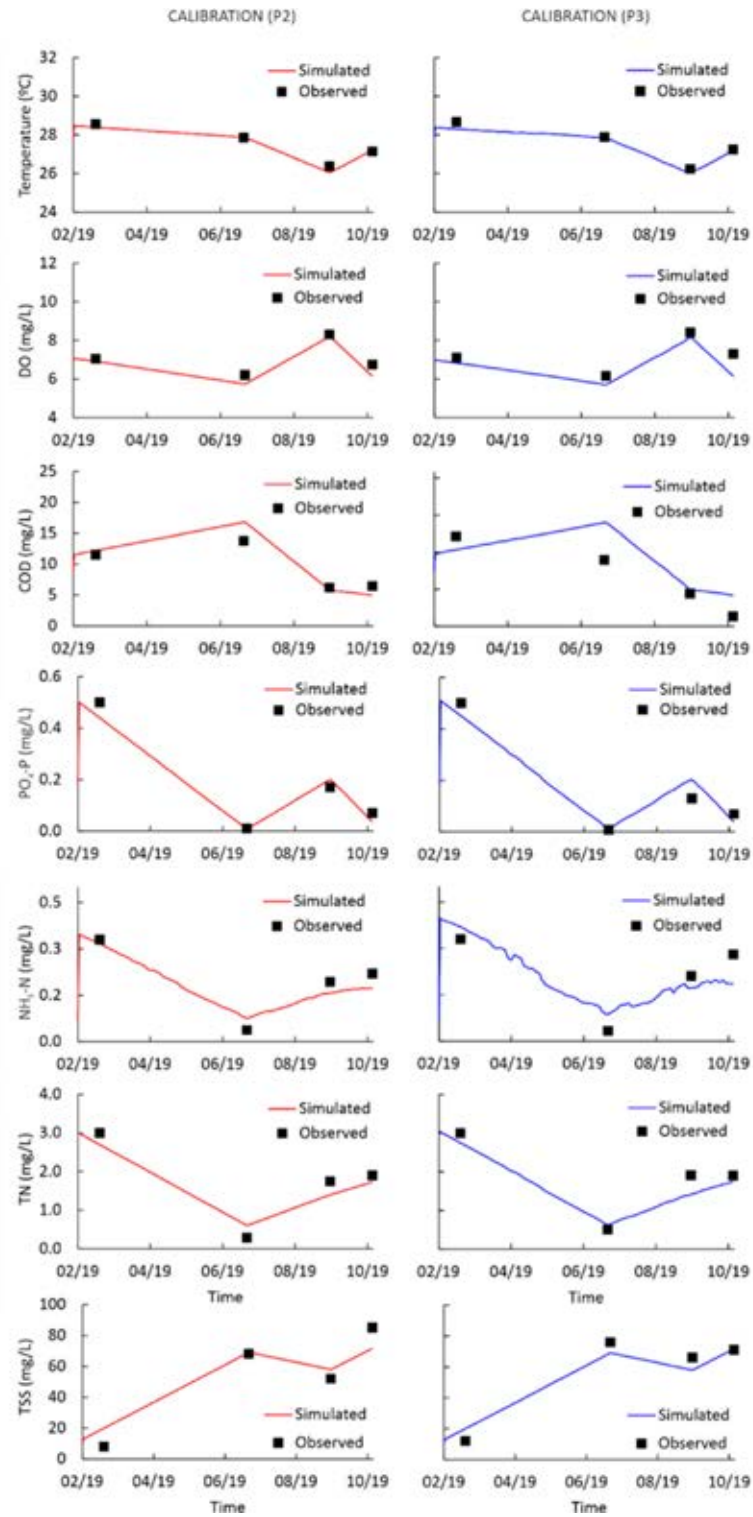

Fig. 5: Calibration and validation of physicochemical parameters at point 2 (red) and point 3 (blue)

Table 5: Main modified coefficients in the water quality component

Parameter	Reaction rates	(Value/d)
DO	Reaeration Rate (k_a)	1
	Nitrification Rate (k_n)	0.07
	Deoxygenation Rate (k_d)	1.5
COD	Oxidation Rate of the chemical oxygen demand (k_o)	0.03
TN	Nitrification Rate (k_n)	0.07
NH_3-N	Hydrolysis Rate of organic nitrogen (k_{hn})	0.08
	Nitrification Rate (k_n)	0.07
SST	Particle settling velocity (w_s)[a]	1.38×10^{-4}
	Sedimentation Rate of suspended solids (k_s)	-
PO_4-P	Hydrolysis Rate of organic phosphorus (k_{hPO})	0.08

[a] in m/d

Table 6: RMSE results for all parameters

Parameters	SD	RMSE	Fit category	SD	RMSE	Fit category
	P2			P3		
Temperature	0.815	0.177	Very good	0.891	0.202	Very good
COD	3.264	1.725	Acceptable	4.955	3.655	Acceptable
DO	0.770	0.38	Acceptable	0.800	0.623	Acceptable
NH_3-N	0.119	0.032	Very good	0.121	0.065	Acceptable
TN	0.964	0.298	Very good	0.887	0.299	Good
PO_4-P	0.189	0.038	Very good	0.191	0.047	Very good
TSS	28.613	9.604	Good	25.791	6.666	Very good

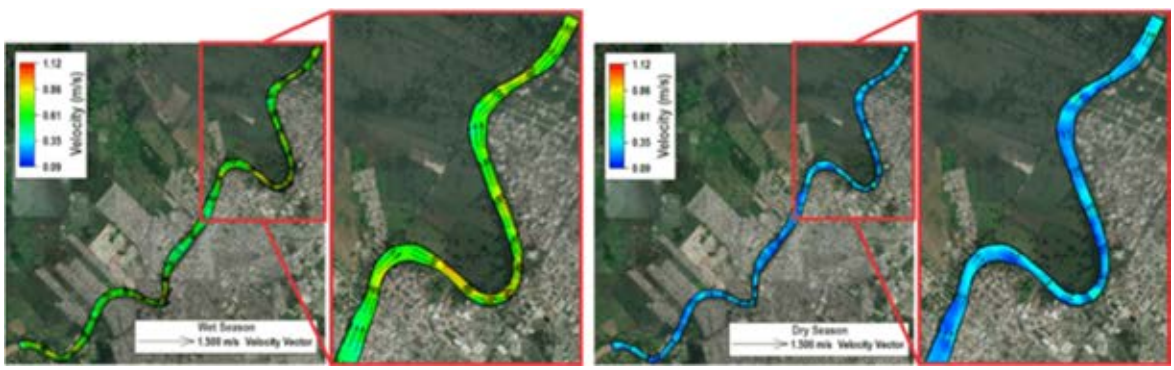

Fig.6: Dry and wet season velocity simulation

season since during wet periods there is a large influx of allochthonous materials into the river through surface runoff, i.e., the movement of rainwater and surface runoff promotes the detachment and entrainment of particles (sediments), increasing TSS (Jaya, 2017; Agustine *et al.*, 2018). Regarding the spatial distribution of concentrations, all parameters were negatively affected in the area immediately after the second discharge (WWTP Northeastern), where it was observed a slight decrease in DO and a significant increase in the other evaluated parameters (COD, NH_3-N, TN, and PO_4-P). This demonstrates the negative impacts that wastewater discharges have on the concentrations of physicochemical parameters in water bodies and their effect on the assimilative capacity of the receiving bodies (Cuesta-Parra *et al.*, 2018). Results relate to Aguilar and Solano, (2018) research regarding the river flow decrease in the dry season that also cause a decrease in de dilution capacity of pollutants from domestic wastewater,

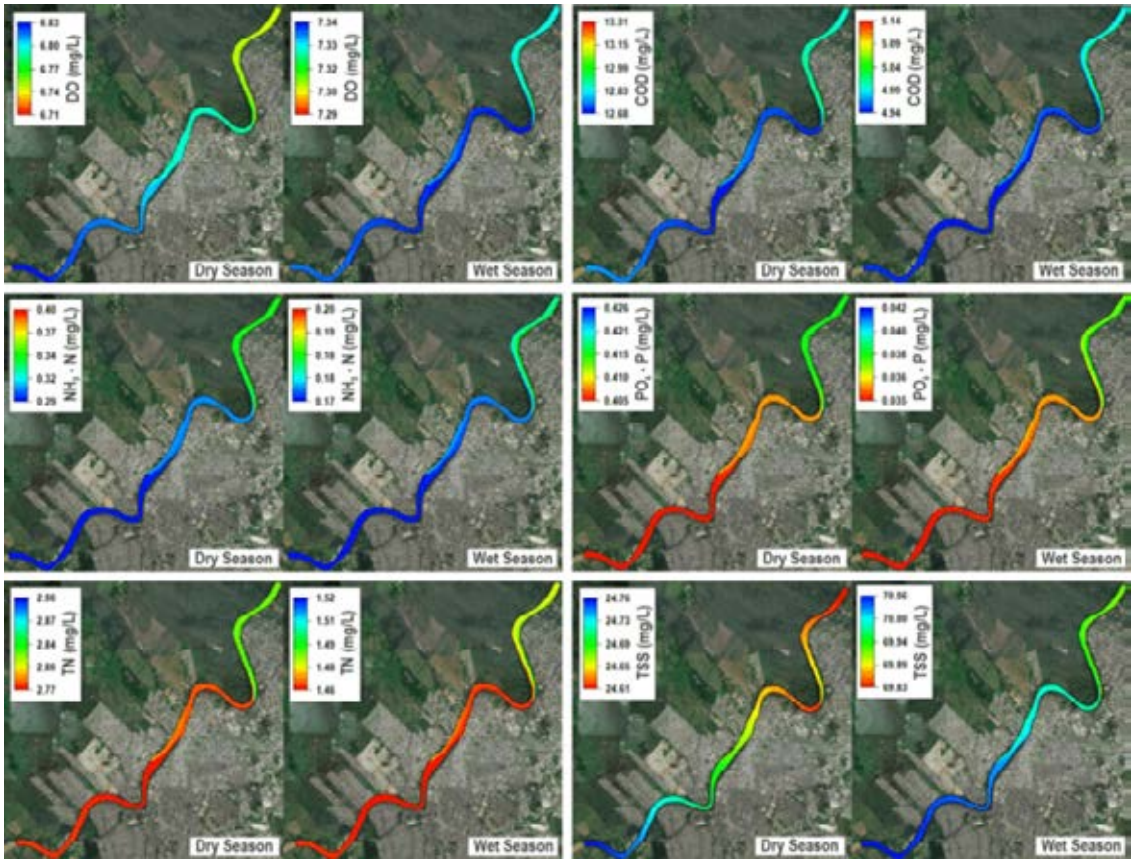

Fig. 7: Simulation results of physicochemical parameters in dry (March 31st) and wet (October 26th) seasons (Note the change of scale in the figures)

therefore affecting the assimilative capacity.

Simulated scenarios and assimilation capacity

Simulation results of the formulated scenarios are shown in Fig. 8. For the evaluation of the assimilation capacity, a comparison between the concentrations in the time series with the established reference limits was carried out.

Temperature

Temperature is a parameter of great importance in the analysis of water quality because its increase in water bodies can produce negative effects on the ecosystem and its fundamental processes, particularly, rivers temperature affects the availability of DO in the water column for fish and other aquatic organisms, it also affects the solubility of chemicals in the water and biological activity (Graham *et al.*, 2014; Zhen-Gang, 2017). Colombian regulations indicate that wastewater discharges must not cause an increase of more than 5 °C in the temperature of surface water bodies; the temperature time series in Fig. 8 shows that none of the scenarios exceeds the reference value, which indicates that the discharges evaluated in the study section do not significantly affect this parameter; however, it should be taken into account that even if the standard is met, the temperature fluctuations predicted in the different scenarios may influence the other water quality parameters studied. S6, which corresponds to a 50 % decrease in river flow and an increase of five times in discharge concentrations and flows, caused the greatest increase in river temperature, reaching 31.7 °C as the maximum value in the dry season; this could negatively affect the river's assimilative capacity since dissolved oxygen concentrations depend also on water temperature (Imam and El Baradei, 2006); an increase in the river's water temperature influences its oxygen metabolism which creates a decrease

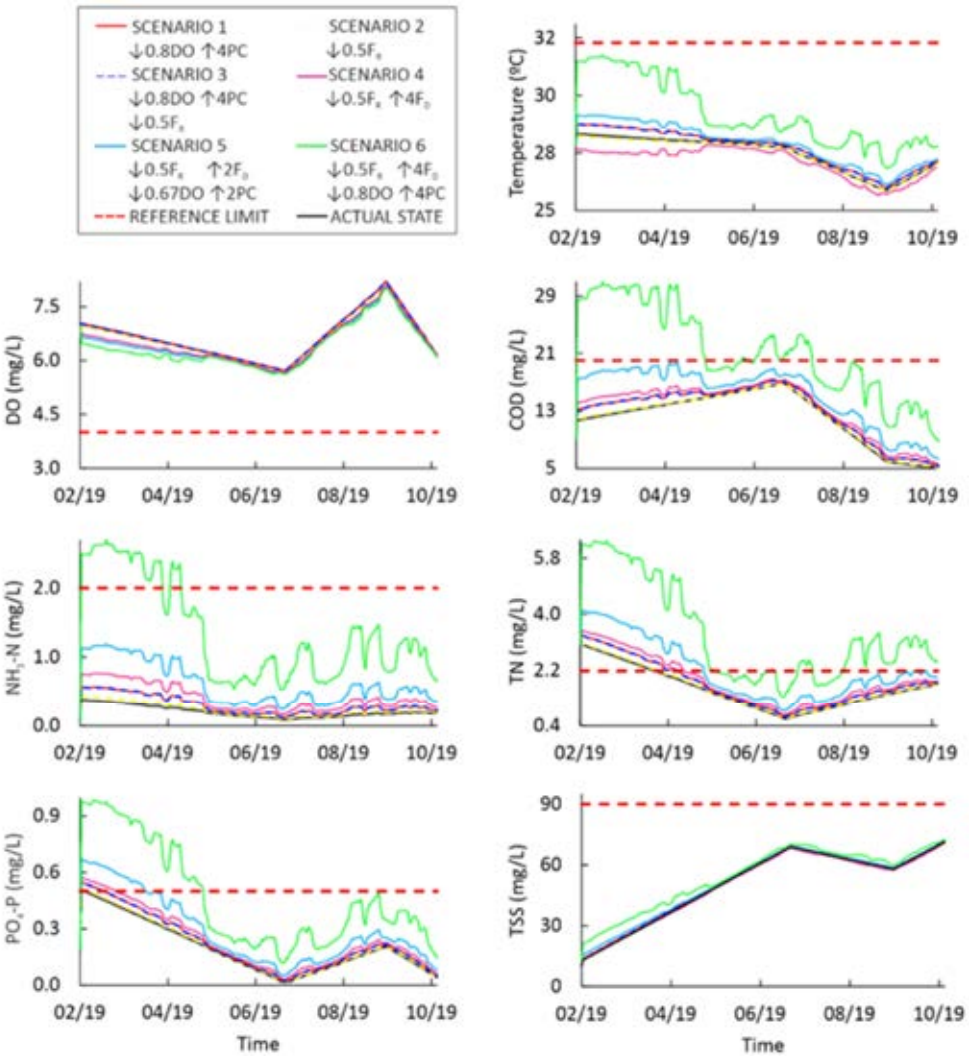

Fig. 8: Time series plots for each parameter

in its assimilative capacity due to rise biochemical processes that deplete oxygen (Chapra *et al.,* 2021).

Chemical Oxygen Demand

COD concentrations in the actual state are higher in March compared to those in October, but the highest concentrations occur between April and May (Fig. 8); however, the graph shows that S6 is the only one that exceeds the reference limit (20 mg/L), this occurs during the first months (March - May) and between June and July; during the dry season this parameter reaches a maximum concentration of 30.9 mg/L and water bodies that exceed the reference limit are considered polluted (Jingsheng *et al.,* 2006; Al-Badaii *et al.,* 2013). These results show that the river's assimilation capacity of this parameter is affected mainly when the river flow decreases by half and the concentrations and flows of discharges increase five times, which are the conditions in S6. In general, the change in flow rates, both in the river and in discharges, is the condition that affects assimilation capacity the most. S5 also shows a considerable increase in this parameter during the dry season, because in this scenario the river flow was reduced by half and the concentrations and flows of discharges increased three times. In all scenarios, a significant decrease

in COD was observed in October. This behavior is similar to the results obtained by Islam *et al.* (2015), where a decrease in COD was also observed during the wet period and an increase during the dry period. According to the results of their research, where there were higher concentrations of COD and NH_3-N in the dry season, Liu *et al.,* (2018) suggest that the reduction of the water assimilative capacity during the dry season showed that the pollution loads in this season were much more serious than the wet season and a reduction in pollutants loads must be done to meet its water quality protective goal.

Dissolved oxygen

Poor water quality is considered when DO concentrations are lower than the reference limit of 4 mg/L, thus it can be harmful to some fish and macroinvertebrate populations and have negative effects on chemical reactions of aquatic ecosystems (Patel and Vashi, 2015). As shown in Fig. 8, DO remains at good levels over this limit throughout the simulation time in all scenarios. Considering the above, it can be said that the river has the capacity to adequately assimilate current discharges without significantly affecting this parameter, therefore the river preserves its ability to assimilate oxygen demanding pollutants without disrupting the aquatic ecosystem (Chapra, 2018), even under the worst conditions represented by S6. In S6's dry season, there was a greater decrease in DO compared to its current state, which is associated with low flow values and less aeration of the medium (Liu *et al.,* 2020). DO decrease in water bodies due to the influence of discharges is consistent with what has been found in different studies (Graham *et al.,* 2014; Rubio *et al.,* 2017).

Ammonia nitrogen and total nitrogen

These parameters' variations are strongly related to both river flow and discharge concentrations and flows. This is evident when observing S2 in Fig. 8, where, although there was a decrease in half of the river flow, the discharge flows and concentrations were not altered, and as a result, concentrations very similar to those of the actual state were obtained. Most significant changes were observed in scenarios S5 and S6, where the flow of the river and the discharges' flow and concentrations were modified. S5 shows that the river can withstand a decrease in its flow by half and an increase of three times in discharge flow and concentrations without exceeding the reference limit for NH_3-N, while the same happens for TN only in the wet season. TN results show that although the reference limit of 2.18 mg/L was exceeded in all scenarios during the first months, by the end of the simulation in the wet season the limit was only exceeded in S6, reaching a maximum TN concentration of 6.3mg/L mg/L, which can accelerate eutrophication processes and generate negative effects on the aquatic ecosystem, as the necessary DO concentration for fish and vegetation could be depleted (Zhen-Gang, 2017). The S6 was the only one where the reference limit of 2 mg/L for NH_3-N was exceeded, and this only occurred in the first simulated months. NH_3-N reached a maximum concentration of 2.7mg/L. These parameters showed a tendency to increase during the dry season, which indicates that the river is not able to assimilate them when the flow is reduced by half and the discharge flow and concentrations increase five times. It is important to keep in mind that in high concentrations ammonia nitrogen can be toxic to aquatic life (Von-Sperling, 2007). These results contrast with those found by Husaini *et al.* (2007), where the highest concentrations were found in the wet season; while in the investigations of Girardi *et al.* (2016); Benjumea *et al.* (2018) and Villota-López *et al.* (2021), higher concentrations were found in the dry season, this is associated with the low dilution due to the decrease in flows during this season. Wang *et al.* (2015) also found that the assimilative capacity in terms of water environmental carrying capacity, tends to be lower for these parameters in the dry season because of the lower water level and degradation ability, while the larger water volume and good dynamic conditions in the wet season were positive to the assimilative capacity.

Phosphates

In general, it can be considered that the river assimilation capacity for this parameter is good because its degradation is observed over time, and at the end of the simulation, the phosphate concentrations are significantly lower than dry season concentrations; this coincides with the general notion that the increase of river flow can decrease the pollutant concentration over time because the dilution and self-purification effects increase;

this happens most frequently when the river's contaminants are mainly from point sources (Meng *et al.,* 2020). Phosphates time series show higher concentrations of this parameter in the dry season (Fig. 8) reaching a maximum concentration of 0.98 mg/L, this is attributed to the increase of pollutants and nutrients concentrations caused by reduced flows and decreased dilution capacity, this may also contribute to algal blooms and decay of DO levels (Montes *et al.,* 2013) especially if the river conditions are those of S6. The most detrimental scenario to the river is S6, since its conditions cause a very significant increase in phosphate concentrations during the dry season, when the reference limit of 0.5 mg/L is exceeded. Scenarios 1, 3 and 4 also show that during the first days of the simulation the limit is exceeded, which indicates that this parameter is sensitive to changes in discharge concentrations, since in scenario 2, where only the river flow decreased, the concentrations varied little compared to the actual state, and did not exceed the limit. During the wet season, phosphate concentrations do not exceed the limit in any of the simulated scenarios. Similar behaviors can be found in several investigations, higher concentrations in the dry season and lower in the wet season (Peña, 2019; Pan *et al*., 2020). Todorova *et al.,* (2017) studied phosphatases as a tool to assess self-purification effectiveness at different types of pollution in running waters since it has a positive correlation with phosphate concentrations and found its great value in terms of wastewater risk identification and evaluation of organic and nutrient loading in streams.

Total suspended solids

Fig. 8 shows that, unlike the other parameters, TSS tend to increase in most months. In the dry season, the concentrations of this parameter are significantly lower than in the wet season, this is associated with the increase of erosion processes during the wet season, this has been evidenced too in different investigations (Agustine *et al.,* 2018; Benjumea *et al.,* 2018). Although the increase of TSS is significant in the wet season, the quality standard of 90 mg/L is not exceeded in any of the scenarios which implies a good assimilation capacity in the river. The Sinú River can assimilate the most extreme conditions (S6), without exceeding the quality standard. On the contrary, in Zubaidah *et al.,* (2018) investigation, TSS loads were higher than the assimilative capacity value causing a detriment in the studied river water quality. TSS analysis is very important for water resource quality studies since it can influence the variability of other parameters. One of its main effects is photosynthetic activity reduction due to light passage loss (Rubio *et al.,* 2017; Cahyono *et al.,* 2019), in the same way, high TSS concentrations suffocate benthic habitats and interfere with feeding activities; additionally, suspended particles promote the absorption of nutrients, organic compounds and other potential pollutants (Graham *et al.,* 2014).

Longitudinal profiles

When analyzing the graphs in Fig. 9, it is found that none of the scenarios show a lower concentration than the reference limit (4 mg/L) for DO. Also, it is observed that in all scenarios DO concentrations during the wet season are higher than in the dry season, which matches with what is reported in the literature, where precipitation has a positive effect on DO (Muñoz *et al*., 2015; Liu *et al.,* 2020). The highest DO concentrations for all scenarios are found upstream of the first discharge (WWTP Southwestern) and the lowest downstream of the second discharge (WWTP Northeastern), with S6 being the scenario that makes oxygen availability vary the most in the two seasons, presenting values higher than 6.04 mg/L in the dry season and 6.79 mg/L in the wet season. DO and COD variability against distance was also investigated by Zubaidah *et al.,* (2019), the diffuse mixture of pollutant loads caused the dissolved oxygen concentration to decrease in downstream points, while the COD increased; however, the self-purification process could take place along the river, mainly in the middle zone of the studied section. Similar findings had Churun *et al.,* (2019) research, the assimilative process was observed in the location with the greater effluent concentration, DO decrease and then showed an increasing trend. Sinú River's results also show a slight decrease of DO immediately after each discharge, but over time, the concentration tends to be higher in the wet season, indicating once again a better assimilative capacity in this season Fig. 9.

In COD's case, none of the scenarios exceeds the established limit concentration (20 mg/L) in the wet season, but in the dry season it is exceeded after the second discharge in S6, presenting a maximum value

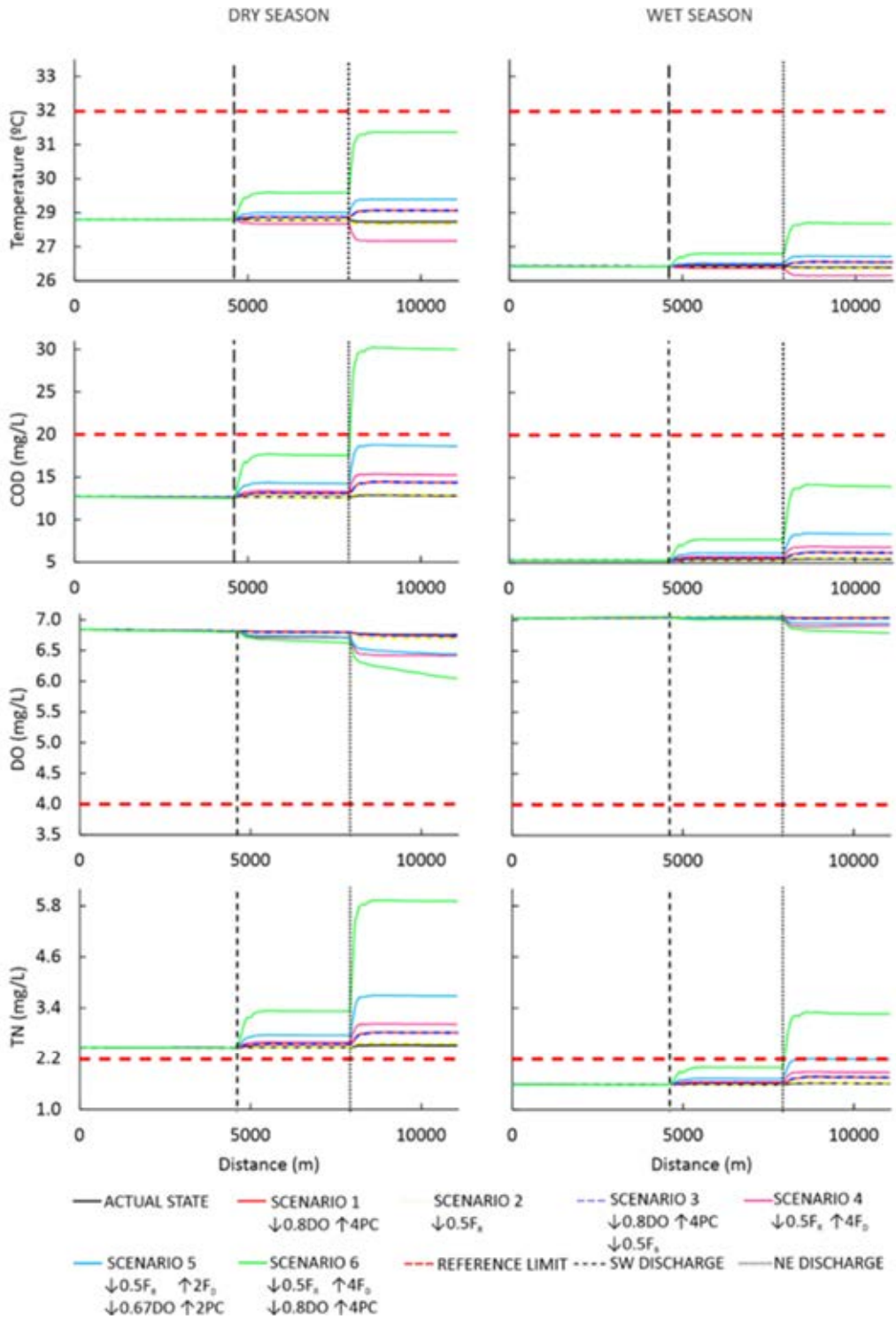

Fig. 9: Longitudinal profiles for temperature, COD, DO y TN

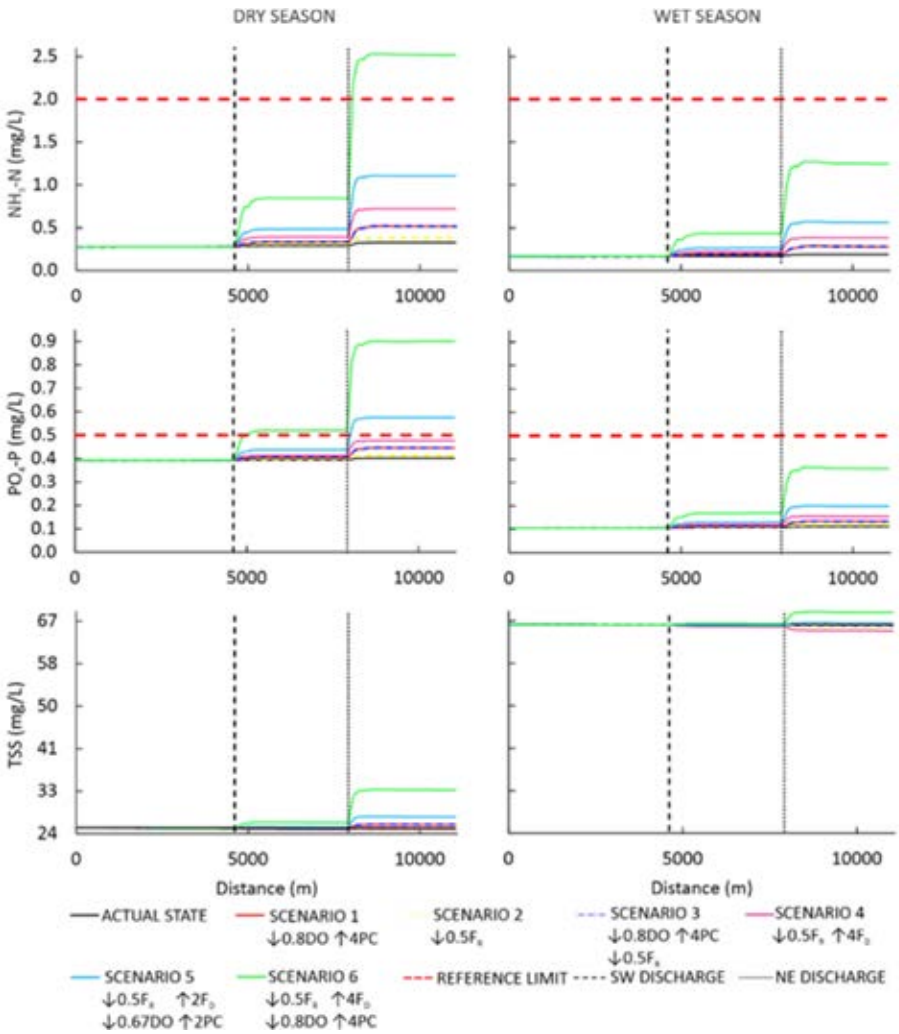

Fig. 10: Longitudinal profiles for PO_4-P, NH_3-N y TSS

of 30.9 mg/L, being this, as well as the DO, the scenario with the greatest variations in COD concentrations. For each scenario, the concentrations in the dry season are higher than during the wet season, as mentioned above, this is because the decrease in flows during the dry season generates a higher concentration of pollutant loads, which causes a decrease in DO and an increase in COD, due to decomposition processes (Liu *et al.,* 2020). It's important to understand that rivers' assimilative capacity is a complex process that also involves the simultaneous work of physical, chemical, and biological processes, and the water pollutants are reduced mostly through biodegradation processes (Taseiko *et al.,* 2016).

In the dry season, all the TN scenarios exceed the reference limit (2.18 mg/L), while in the wet season only S5 and S6 exceed it after the WWTP Northeastern discharge (Fig. 9), with a maximum value of 2.19 mg/L for S5 and 3.31 mg/L for S6. For all scenarios, TN concentrations are also higher during the dry season than the wet season, with greater variations after the wastewater discharges and especially after the second discharge (WWTP Northeastern). S6 is the scenario with the greatest variability in both periods. This situation also occurs for N-NH_3 and PO_4-P. Benjumea *et al.* (2018), found similar results for TN, NH_3-N and PO_4-P, and suggested that it was due to a high presence of organic matter and that the

low flow in the dry season does not allow dilution of these nutrients, in consequence, a lower assimilative capacity is shown. In addition, Toja *et al.* (2003) found higher concentrations of nitrogen and phosphates in low water levels in the Agrío and Guadimar rivers in Spain, attributing the low discharges dilution to the low rivers flow. Comparable results are shown in Meng *et al.*, (2020), rivers' concentration in their study area fluctuates during the research period, these parameters increase first and then decrease due to the pollutant assimilation, and this also happens in Sinú River. Temperature has higher concentrations during the dry season than during the wet season. Meanwhile, the TSS show higher concentrations in the wet season than in the dry season since rainwater movement and surface runoff promote sediments detachment and dragging. Like previous parameters, the greatest variations in concentration occur after the discharges, especially after the Northeastern discharge. Unlike the other parameters, which in all scenarios after the discharges there was only an increase (TN, NH_3-N, COD, PO_4-P) or only a decrease (DO) in the concentrations obtained in the simulations, this was not the case for temperature and TSS, because while in scenarios S1, S3, S5 and S6 their concentrations increased, in scenarios S2 and S4 their concentrations decreased after the discharges. It should be noted that for S2 and S4 there was no change in discharge concentrations, only in flow rates.

CONCLUSION

EFDC Explorer hydrodynamic and water quality model implementation showed an adequate fit of the measured data compared to those calculated by the model, especially for river water level, temperature, phosphates and total nitrogen, giving confidence in the model's adaptability to the river hydrodynamic and water quality conditions. For this reason, its use become one of the main tools for the Sinú River basin management and provide a bigger approach regarding Sinú River assimilative capacity. Model spatiotemporal simulations and the evaluated scenarios showed the discharges' effect on Sinú River's assimilative capacity since some parameters (TN, NH_3-N, COD, PO_4-P) exceeded the established reference levels and these are relevant to meet the necessary water quality criteria to keep a healthy aquatic ecosystem. It was possible to evaluate the assimilative capacity over time, observing a better assimilation for parameters such as COD, DO, PO_4-P, TN and NH_3-N during the wet season than the dry season. In general, it can be considered that Sinú River's assimilation capacity is good over time. In addition, it was found that Sinú River is more sensitive to changes in discharge flows than changes in discharge concentrations, the river was mostly affected by the decrease of its flow in half, and the 400% increase in current point sources flows; this notion can influence the river's planning and prevention programs in terms of wastewater flows that can be supported by the river without depleting its assimilative capacity; since this aspect is not currently taken into consideration for its management. Sinú River water quality modeling serves as a starting point for the competent environmental authorities to evaluate the river's self-purification ability under the current discharge conditions and predict which conditions this natural process gets affected; it constitutes a fundamental tool for the planning, design, and implementation of water resource pollution control programs and the development of effective water quality objectives.

AUTHOR CONTRIBUTIONS

F. Torres-Bejarano performed the experimental design, sampling campaigns, water quality analysis, and prepared the manuscript text. M. Verbel-Escobar performed the literature review and the model configuration and simulations, analyzed, and interpreted the data and results. M.C. Atencia-Osorio organized the methodology, analyzed, and interpreted the data and results, prepared the manuscript text, and manuscript edition.

ACKNOWLEDGEMENT

Authors are grateful to the University of Córdoba and especially to the Environmental Engineering Program for the support provided to carry out this investigation project.

CONFLICT OF INTEREST

The authors declare no potential conflict of interest regarding the publication of this work. In addition, the ethical issues including plagiarism, informed consent, misconduct, data fabrication and, or falsification, double publication and, or submission, and redundancy have been completely witnessed by the authors.

ABBREVIATIONS

^oC	Degree Celsius
AS	Actual state
A_b	Vertical turbulent eddy viscosity
AC	Assimilative capacity
A_H	Horizontal momentum and mass diffusivity
A_H	Horizontal turbulent eddy diffusivity
ANC_x	Nitrogen-carbon ratio constant in algal group *x*
AOCR	Dissolved oxygen to carbon ratio in respiration
AONT	Mass of dissolved oxygen consumed per unit mass of ammonium nitrogen nitrified
APC	Mean algal phosphorus-to-carbon ratio for all algal groups
Aut	Automatic
A_v	Vertical turbulent eddy viscosity
BFCOD	Sediment flux of chemical oxygen demand
$BFNH_4$	Water-sediment ammonium flux exchange
BFPO4d	Sediment-water exchange flux of phosphate
BM_x	Basal metabolism rate of algal group *x*
B_x	Algal biomass of algal group *x*
C	Concentration or intensity of transport constituent
C_j	represents the concentration of the j^{th} sediment class
COD	Chemical oxygen demand
c_p	Vegetation resistance coefficient
CVS	Regional Autonomous Corporation of the Sinú and San Jorge Valleys
d	Day
DO	Dissolved oxygen
DO	Dissolved oxygen concentration (equation)
DOC	Concentration of dissolved organic carbon
DON	Dissolved organic nitrogen concentration
DOP	Dissolved organic phosphorus concentration
DO_s	Saturated concentration of dissolved oxygen
D_p	Projected vegetation area normal to the flow per unit horizontal area
DWTP	Drinking water treatment plant
DX	Distance on the *X* axis
DY	Distance on the Y axis
EFDC	Environment Fluid Dynamics Code
F	Flow
f	Coriolis parameter
FCD_x	Fraction of basal metabolism exuded as dissolved organic carbon
F_D	Discharge flow
FNIP	Fraction of nitrogen produced and stripped as inorganic nitrogen
FNI_x	Fraction of nitrogen metabolized by algal group *x* produced as inorganic nitrogen

FPIP	Fraction of predated phosphorus produced as inorganic phosphorus
F_R	River flow
H	Total depth
h	Water depth bellow the vertical reference level
i	Cell
IDEAM	Institute of Hydrology, Meteorology and Environmental Studies
IWA	International water association
k_a	Reaeration Rate
K_{COD}	oxidation rate of chemical oxygen demand
k_d	Deoxygenation Rate
K_{DON}	Rate of dissolved organic nitrogen mineralization
K_{DOP}	Dissolved organic phosphorus mineralization rate
KH_{COD}	Half-saturation constant of dissolved oxygen required for oxidation of *COD*
k_{hn}	Hydrolysis Rate of organic nitrogen
k_{hPO}	Hydrolysis Rate of organic phosphorus
K_{HR}	Heterotrophic respiration rate of dissolved organic carbon
KHR_x	Half-saturation constant of dissolved oxygen for algal dissolved organic carbon excretion for group *x*
km	Kilometer
K_{Nit}	Nitrification rate
K_R	Reaeration coefficient
k_s	Sedimentation Rate of suspended solids
L	Liter
m	Meter
mg	Milligram
mm	Millimeter
m_x	Square roots of the diagonal components of the metric tensor
m_y	Square roots of the diagonal components of the metric tensor
N	North
N	Sample size
NC	No change
NE	Northeastern
NH_3-*N*	Ammonia nitrogen
NH_4	Ammonium nitrogen concentration
NOAA	National Oceanic and Atmospheric Administration
O_i	Measured data
p	Physical pressure in excess of the reference density hydrostatic pressure
P1	Monitoring point 1
P2	Monitoring point 2
P3	Monitoring point 3
P4	Monitoring point 4
P_{atm}	Barotropic pressure
PC	Physicochemical
P_i	Simulated data
PN_x	preference for ammonium uptake by algal group *x*
PO4d	Dissolved phosphate
PO4p	Particulate (sorbed) phosphate
PO_4-*P*	Phosphates
PO4t	Total phosphate concentration
PR_x	Predation rate of algal group
RMSE	The Root Mean Square
s	Second
S1	Scenario 1
S2	Scenario 2
S3	Scenario 3
S4	Scenario 4
S5	Scenario 5
S6	Scenario 6
S_c	Internal and external sources and sinks per unit volume
SD	Standard deviation
$S^E_{s,j}$	external source-sink term
$S^I_{s,j}$	Internal source-sink term

SOD	Sediment oxygen demand, applied to the bottom layer only
S_u	Source/sink term for the horizontal momentum in the x direction
S_v	Source/sink term for the horizontal momentum in the y direction
SW	Southwestern
T	Temperature
t	Time
TN	Total nitrogen
TSS	Total suspended solids
u	Horizontal velocity components in the curvilinear coordinate
US EPA	United States Environmental Protection Agency
v	Horizontal velocity components in the curvilinear coordinate
V	Cell volume
VIMS	Virginia Institute of Marine Science
W	West
w	Vertical velocity component
w_s	Particle settling velocity
WCOD	External loads of chemical oxygen demand
WNH_4	External ammonium loads
WOD	External loads of dissolved oxygen
WPO4t	External loads of total phosphate
WS_{TSS}	Sedimentation rate of the suspended solid
WWTP	Wastewater treatment plant
x	Orthogonal curvilinear coordinates in the horizontal direction
y	Orthogonal curvilinear coordinates in the horizontal direction
ζ	Water surface elevation above the vertical reference level
ρ	Water density

REFERENCES

Acosta, K., (2013). La economía de las aguas del río Sinú. Banco de la República - Center for Regional Economic Studies (CEER). Cartagena. 194: 17 -39 **(23 pages)**.

Aguilar, S.; Solano, G., (2018). Evaluación del impacto por vertimientos de aguas residuales domésticas, mediante la aplicación del índice de contaminación (ICOMO) en Caño Grande, localizado en Villavicencio-Meta. Bachelor's Thesis, Santo Tomás University, Colombia **(80 pages)**.

Agustine, A.; Wuana, R.A.; Silas, I., (2018). Seasonal variation in water quality parameters of river Mkomon Kwande local government area, Nigeria. Int. J. Recent Res. Phys. Chem. Sci., 5(1): 42-62 **(21 pages)**.

Al-Badaii, F.; Shuhaimi-Othman, M.; Gasim, M.B., (2013). Eater quality assessment of the Semenyih river, Selangor, Malaysia. J. Chem., 2013: 1–10 **(10 pages)**.

Benjumea Hoyos, C.A.; Suárez-Segura, M.A.; Villabona-González, S.L., (2018). Temporary and spatial variation of nutrients and total suspended solids in the basin of a high mountain tropical river. Rev. Academia Colomb. Cienc. Exactas, Fis. y Naturales. 42(165): 353–363 **(11 pages)**.

Cahyono, B.E.; Jamilah, U.L.; Misto; Nugroho, A.T.; Subekti, A., (2019). Analysis of total suspended solids (TSS) at Bedadung River, Jember District of Indonesia using remote sensing Sentinel 2A data. Singapore J. Sci. Res., 9: 117-123 **(7 pages)**.

Cely-Calixto, N.J.; Bonilla-Granados, C.A.; Carrillo Soto, G.A., (2021). A mathematical model for the simulation of the Magdalena River in the city of Barrancabermeja, Colombia. J. Phys. Conf. Ser., 1981: 012016 **(7 pages)**.

Chapra, S.C., (2018). Advances in river water quality modelling and management: Where we come from, where we are, and where we're going? Green energy and technology. Springer: 295–301 **(7 pages)**.

Chapra, S.C.; Camacho, L.A.; McBride, G.B., (2021). Impact of global warming on dissolved oxygen and BOD assimilative capacity of the world's rivers: Modeling analysis. Water, 13(17): 2408 **(20 pages)**.

Churun, A.; Siti, R.; Haeruddin; Heppi Puspita, S. (2019). Purification capacity and oxygen sag in Sringin River, Semarang. Int. J. Appl. Environ. Sci., 14(1): 1-16 (**16 pages**).

Cuesta-Parra, D.; Velazco-Rincón, C.; Castro-Pardo, J., (2018). Environmental assessment related to the sewage water discharge of a tannery company into Aburrá River. Rev. UIS Ing., 17(2): 141–151 **(11 pages)**.

CVS, (2004). Plan de ordenamiento y manejo de cuencas hidrográficas del río Sinú. Diagnóstico ambiental de la cuenca hidrográfica del río Sinú. Montería, Colombia **(88 pages)**.

Dehghani Darmian, M.; Khodabandeh, F.; Azizyan, G.; Giesy, J.P.; Hashemi Monfared, S.A., (2020). Analysis of assimilation capacity for conservation of water quality: controllable discharges of pollutants. Arabian J. Geosci., 13: 888 **(13 pages)**.

DSI, (2020). EFDC+ Theory Document. Version 10.2. Edmonds, United States **(284 pages)**.

Egbe, J.G.; Agunwamba, J.C.; Okon, E.E., (2018). Modeling and modification of the effect of self purification of Kwa river pollution. Int. J. Curr. Res. Acad. Rev., 6(9): 83-89 **(7 pages).**

Feria Díaz, J.J.; Náder Salgado, D.; Meza Pérez, S.J., (2017). Deoxygenation and re-aeration rates of the Sinu river. Ing. Desarrollo, 35(1): 1-17 **(17 pages)**.

Girardi, R.; Pinheiro, A.; Pospissil, L.; Torres, É., (2016). Water quality change of rivers during rainy events in a watershed with different land uses in Southern Brazil. Braz. J. Water Resour., 21(3): 514–524 **(11 pages)**.

Graham, J.L.; Stone, M.L.; Rasmussen, T.J.; Foster, G.M.; Poulton, B.C.; Paxson, C.R.; Harris, T.D., (2014). Effects of wastewater effluent discharge and treatment facility upgrades on environmental and biological conditions of Indian Creek, Johnson County, Kansas, June 2004 through June 2013: U.S. Geological Survey Scientific Investigations Report 2014–5187 **(92 pages).**

Gurjar, S.K.; Tare, V., (2019). Spatial-temporal assessment of water quality and assimilative capacity of river Ramganga, a tributary of Ganga using multivariate analysis and QUEL2K. J. Cleaner Prod., 222: 550–564 **(15 pages).**

Hashemi Monfared, S.A.; Dehghani Darmian, M.; Snyder, S.A.; Azizyan, G.; Pirzadeh, B.; Moghaddam, M.A., (2017). Water quality planning in rivers: assimilative capacity and dilution flow. Bull. Environ. Contam. Toxicol., 99(55): 531–541 **(11 pages)**.

Husaini, C.; Gbodi, A.; Orisakwe, O.; Ogbadoyi, E.; Ali, J.; Hussaini, M.; Garba, S.; Afonne, J.; Pam, H., (2007). Seasonal nitrate content of stream water, soil and some foodstuffs samples in Abuja municipal area of Federal Capital Territory, Nigeria. J. Health Sci., 53(4): 359–364 **(6 pages)**.

Imam, E.; El Baradei, S., (2006). Ecosystem and assimilative capacity of rivers with control structures. WIT Trans. Ecol. Environ., 95: 435 – 444 **(10 pages)**.

Islam, M.S.; Uddin, M.K.; Tareq, S.M.; Shammi, M.; Kamal, A.K.I.; Sugano, T.; Kurasaki, M.; Saito, T.; Tanaka, S.; Kuramitz, H., (2015). Alteration of water pollution level with the seasonal changes in mean daily discharge in three main rivers around Dhaka City, Bangladesh. Environ., 2(3): 280–294 **(15 pages).**

IDEAM, (2017). Protocolo de monitoreo del agua. Bogotá, D. C., Colombia **(587 pages).**

IWA, (2018). Wastewater Report 2018. The Reuse Opportunity. **(24 pages).**

Jaya, F., (2017). Estudio de los sólidos suspendidos en el agua del rio Tabacay y su vinculación con la cobertura vegetal y usos del suelo en la microcuenca. Bachelor's Thesis Cuenca University, Ecuador **(103 pages).**

Jingsheng, C.; Tao, Y.; Ongley, E., (2006). Influence of high levels of total suspended solids on measurement of COD and BOD in the Yellow river, China. Environ. Monit. Assess., 116: 321–334 **(14 pages)**.

Kim, J.; Lee, T.; Seo, D., (2017). Algal bloom prediction of the lower Han River, Korea using the EFDC hydrodynamic and water quality model. Ecol. Modell., 366: 27-36 **(10 pages).**

Kulikova, D.; Kovrov, O.; Buchavy, Y.; Fedotov, V., (2018). GIS-based Assessment of the Assimilative Capacity of Rivers in Dnipropetrovsk Region. J. Geol. Geogr. Geoecol., 27(2): 274-285 **(12 pages)**.

Lee, I.; Hwang, H.; Lee, J.; Yu, N.; Yun, J.; Kim, H., (2017). Modeling approach to evaluation of environmental impacts on river water quality: A case study with Galing River, Kuantan, Pahang, Malaysia. Ecol. Modell., 353: 167-173 **(7 pages)**.

Liu, G.; He, W.; Cai, S., (2020). Seasonal variation of dissolved oxygen in the southeast of the Pearl River estuary. Water. 12: 2475 **(18 pages)**.

Liu, Q.; Jiang, J.; Jing, C.; Qi, J., (2018). Spatial and seasonal dynamics of water environmental capacity in mountainous rivers of the Southeastern Coast, China. Int. J. Environ. Res. Public Health. 15(1): 99 **(21 pages)**.

Meng, Chunfang; Song, Xiaoyu; Tian, Kening; Ye, Bingxiao; Si, Tianxiu, (2020). Spatiotemporal variation characteristics of water pollution and the cause of pollution formation in a heavily polluted river in the upper Hai River. J. Chem., 2020: **(15 pages).**

Montes, R.; Navarro, I.; Domínguez, R.; Jiménez, B., (2013). Modificación de la capacidad de autodepuración del río Magdalena ante el cambio climático. Tecnol. Cienc. Agua, 4(5): 71-83 **(13 pages)**.

Muñoz, H.; Orozco, S.; Vera, A.; Suárez, J.; García, E.; Neria, M.; Jiménez, J., (2015). Relationship between dissolved oxygen, rainfall and temperature: Zahuapan River, Tlaxcala, Mexico. Tecnol. Cienc. Agua, 6(5): 59-74 **(16 pages)**.

Novo, P., (2017). Accounting for the assimilative capacity of water systems in Scotland. Water, 9(8): 559 **(13 pages)**.

Obin, N.; Tao, H.; Ge, F.; Liu, X., (2021). Research on water quality simulation and water environmental capacity in Lushui river based on WASP model. Water, 13(20): 2819 **(20 pages)**.

Pan, L.; Dai, J.; Wu, Z.; Wan, Z.; Zhang, Z.; Han, J.; Li, Z.; Xie, X.; Xu, B., (2020). Spatio-temporal dynamics of riverine nitrogen and phosphorus at different catchment scales in Huixian Karst Wetland, Southwest China. Water, 12(10): 2924 **(23 pages)**.

Patel, H.; Vashi, R.T., (2015). Chapter 2 - Characterization of textile wastewater. Characterization and treatment of textile wastewater, Elsevier Inc. 21–71 **(51 pages)**.

Peña, D., (2019). Diagnóstico de la calidad del agua de la Microcuenca quebradas las delicias cerros orientales de Bogotá a partir de los parámetros químicos de acuerdo con la normativa legal vigente. Bachelor's Thesis, Cooperative University of Colombia **(77 pages)**.

Quinn, N.W.T.; Tansey, M.K.; Lu, J., (2021). Comparison of deterministic and statistical models for water quality compliance forecasting in the San Joaquin river basin, California. Water, 13(19): 2661 **(32 pages)**.

Ramos, L.Á., (2018). Estudio de la dinámica del cromo en la cuenca alta del río Bogotá mediante la selección y aplicación de un modelo de calidad de agua para la representación de contaminantes conservativos en cuerpos de agua lóticos. Bachelor's Thesis, National Open and Distance University, UNAD Institutional Repository **(131 pages)**.

Ritter, A.; Muñoz-Carpena, R., (2013). Performance evaluation of hydrological models: Statistical significance for reducing subjectivity in goodness-of-fit assessments. J. Hydrol., 480: 33–45 **(13 pages)**.

Rubio, A.; Amézquita, L.; Martínez, E., (2017). Determinación de la capacidad de asimilación del vertimiento de la PTAR del municipio de Tenjo, Cundinamarca en la quebrada Churuguaco mediante el modelo QUAL2KW. Water Resources Specialization, Universidad Católica De Colombia **(161 pages)**.

Taseiko, O.; Spitsina, T.P.; Milosevic, H.; Radavanovic, D.; Valjarevic, A., (2016). Biochemical processes of self-purification model in small rivers. Math. Inf. Technol., 487 – 495 **(9 pages).**

Todorova, Y.; Schneider, I.; Yotinov, I.; Lincheva, S.; Topalova, Y., (2017). Potential of phosphatases for express assessment of self-purification at different types of pollution in running waters. Water Pract. Technol., 12(4): 953–963 **(11 pages).**

Torres-Bejarano, F.; Padilla Coba, J.; Rodríguez-Cuevas, C.; Ramírez-León, H.; Cantero-Rodelo, R., (2016). The hydrodynamic modelling for the water management of el Guájaro Reservoir, Colombia. Rev. Int. Metodos Numer. Calc. Diseno Ing., 32(3): 163-172 **(10 pages)**.

Torres-Bejarano, F.; Torregroza-Espinosa, A.; Martinez-Mera, E.; Castañeda-Valbuena, D.; Tejera-Gonzalez, M. (2020). Hydrodynamics and water quality assessment of a coastal lagoon using environmental fluid dynamics code explorer modeling system. Global J. Environ. Sci. Manage., 6(3): 289-308 **(20 pages)**.

Toja, J.; Alcalá, E.; Burgos, M.D.; Martín, G.; Plazuelo, A.; Schutter, T.; Prat, N.; Plans, M; Solá, C., (2003). Efecto del vertido tóxico en las comunidades de plancton y perifiton del río Guadiamar. Ministry of Environment. Regional Government of Andalusia **(16 pages)**.

Valbuena, D., (2017). Geomorfología y condiciones hidráulicas del sistema fluvial del rio Sinú. Integración multiescalar 1945 - 1999 - 2016. Master's Thesis, Colombia National University, Bogotá, Colombia **(21 pages)**.

Villota-López, C.; Rodríguez-Cuevas, C.; Torres-Bejarano, F.; Cisneros-Pérez, R.; Cisneros-Almazán, R.; Couder-Castañeda, C., (2021). Applying EFDC Explorer model in the Gallinas River, Mexico to estimate its assimilation capacity for water quality protection. Sci. Rep., 11(1): 13023 **(16 pages)**.

Von-Sperling, M., (2007). Wastewater Characteristics, Treatment and Disposal. IWA Publishing Volume 1 **(306 pages)**.

Wang, H.; Zhou, Y.; Tang, Y.; Wu, M.; Deng, Y., (2015). Fluctuation of the water environmental carrying capacity in a Huge River-Connected Lake. Int. J. Environ. Res. Public Health, 12(4): 3564–3578 **(15 pages)**.

Yiping, Li.; Kumud, Acharya.; Zhongbo, Yu., (2011). Modeling impacts of Yangtze River water transfer on water ages in Lake Taihu, China. Ecol. Eng., 37(2): 325-334 **(10 pages).**

Yuceer, M.; Coskun, M.A., (2016). Modeling water quality in rivers: A case study of Beylerderesi River in Turkey. Appl. Ecol. Environ. Res., 14(1): 383-395 **(13 pages).**

Zhen-Gang, J., (2017). Hydrodynamics and water quality: modeling Rivers, lakes, and estuaries. Second Edition, John Wiley & Sons Inc **(577 pages).**

Zubaidah, T.; Karnaningroem, N.; Slamet, A., (2018). Pollutant load and assimilation capacity in Martapura river, South Kalimantan, Indonesia. Built Environ. Sci. Technol. Int. Conf., 226-229 **(4 pages).**

Zubaidah, T.; Karnaningroem, N.; Slamet, A., (2019). The self-purification ability in the rivers of Banjarmasin, Indonesia. J. Ecol. Eng., 20(2): 177-182 **(6 pages)**.

AUTHOR (S) BIOSKETCHES

Torres-Bejarano, F., Ph.D., Associate Professor, Departament of Environmental Engineering, University of Córdoba, Carrera 6 No. 77-305, Montería, Colombia.
- Email: franklintorres@correo.unicordoba.edu.co
- ORCID: 0000-0003-3144-7289
- Web of Science ResearcherID: AAB-6324-2022
- Scopus Author ID: 22955027500
- Homepage: https://www.researchgate.net/profile/Franklin-Torres-Bejarano/

Verbel-Escobar, M., B.Sc., Environmental Engineering Program, University of Córdoba, Carrera 6 No. 77- 305, Montería, Colombia.
- Email: mverbelescobar73@correo.unicordoba.edu.co
- ORCID: 0000-0002-7350-9890
- Web of Science ResearcherID: NA
- Scopus Author ID: NA
- Homepage: https://38.academia.edu/MelanieVerbelEscobar

Atencia-Osorio, M.C., B.Sc., Environmental Engineering Program, University of Córdoba, Carrera 6 No. 77- 305, Montería, Colombia.
- Email: matenciaosorio39@correo.unicordoba.edu.co
- ORCID: 0000-0001-8482-0687
- Web of Science ResearcherID: NA
- Scopus Author ID: NA
- Homepage: https://unicordoba.academia.edu/MariaCamila97

HOW TO CITE THIS ARTICLE

Torres-Bejarano, F.; Verbel-Escobar, M.; Atencia-Osorio, M.C., (2022). Water quality model-based methodology to assess assimilative capacity of wastewater discharges in rivers. Global J. Environ. Sci. Manage., 8(4): 449-472.

DOI: 10.22034/gjesm.2022.04.01

url: https://www.gjesm.net/article_249277.html